**Steel and Composite Structures**, *Vol. 35, No. 1* (*2020*) *13-27*
DOI: https://doi.org/10.12989/scs.2020.35.1.013


# Stress-strain model of weak PVC-FRP confined concrete column and strong RC ring beam joint under eccentric compression

Feng Yu[a], Nannan Zhang[b], Yuan Fang*, Jie Liu[c] and Guosheng Xiang[d]

*Department of Civil engineering and Anhui University of Technology, Maxiang Road 59, Maanshan, China*

(*Received September 24, 2019, Revised December 27, 2019, Accepted January 4, 2020*)

**Abstract.** To investigate the stress-strain relation of PVC-FRP Confined Concrete (PFCC) column with RC ring beam joint subjected to eccentric compression, the experiment of 13 joint specimens, which were designed with principle of "strong joint and weak column", were presented. Several variable parameters, such as reinforcement ratio, width and height of ring beam, FRP strips spacing and eccentricity, were considered. The specimens were eventually damaged by the crushing of concrete, the fracture of PVC tube and several FRP strips. With the FRP strips spacing or eccentricity increased, the ultimate carrying capacity of specimens declined. The strain of FRP strips and axial strain of PVC tube decreased as FRP strips spacing decreased. The decrease of eccentricity would slow down the development of strain of FRP strips and axial strain of PVC tube. The slope of stress-strain curve of PFCC column decreased as FRP strips spacing or eccentricity increased. The ultimate strain of PFCC column reduced as FRP strips spacing increased, while the effect of eccentricity on the ultimate strain of PFCC was not distinct. Considering the influence of eccentricity on the stress-strain relation, a modified stress-strain model for conveniently predicting the weak PFCC column and strong RC ring beam joint under eccentric compression was proposed and it was in good agreement with the experimental data.

**Keywords:** stress-strain relation; eccentric compression; carrying capacity; PVC-FRP; column; beam; joint

## 1. Introduction

FRP had the advantages of high strength, light weight, fatigue resistance, and good durability, and it was increasingly used in structures (Abdelkarim *et al.* 2017, Attari and Tavakkolizadeh 2019, Dhahir and Kareem 2017, Gholampour and Ozbakkaloglu 2017, Grammatikou *et al*. 2018, Liang, *et al*. 2019, Prashob *et al*. 2019, Xie *et al.* 2019, Chen and Wang 2019, Mansouri 2015, Ozbakkaloglu *et al*. 2013, Teng *et al*. 2009, Ozbakkaloglu and Lim 2013, Wei and Wu 2012, Harajli 2006, Mansouri 2016). Meanwhile, PVC material was also extensively applied due to its merits of cheap, fatigue resistance, and environmental protection. As early as in 1978, Kurt (1978) first poured concrete into a PVC tube to form a novel composite structure-the PVC confined concrete (PCC) column. The ductility of this PCC column was remarkably improved.

To take full advantage of the above-mentioned PVC and FRP, Saafi (2001) proposed a grooved PFCC column. This column not only improved the carrying capacity but also significantly enhanced the ductility of the specimen. However, the stress concentration was easy to occur at the grooved position. To overcome this problem, Yu (2007) simplified the construction process of PVC-FRP tube, and winded the FRP strips directly on PVC tube. A new non-grooved PFCC column including steel skeleton, core concrete and PVC-FRP tube was proposed. In comparison, this new composite column is more economical and has better long-term stability than the well-researched FRP confined concrete column.

So far, some scholars had made a lot of achievements on the study of static behavior, seismic performance and durability of PFCC columns (Niu *et al*. 2017, Yu *et al.* 2018, Toutanji and Saafi 2002). Among them, Fakharifar (Fakharifar and Chen 2016), and Yu (2007) conducted the axial compression experiments on PFCC columns and the test results indicated that the carrying capacity and ductility of the PFCC columns were notably improved. (Yu *et al* 2015, Niu *et al*. 2017, Yu 2014) conducted an experiment on the PFCC column under eccentric load. Results revealed that with the increment of eccentricity or FRP strips spacing, the carrying capacity of the eccentrically loaded PFCC column decreased. (Fakharifar and Chen 2017) studied the flexural behavior of PFCC columns and indicated that the FRP strips could effectively improve the flexural capacity of the PFCC columns. Chen (2016) and Jiang *et al.* (2014) carried out the experiments on seismic behavior of PFCC column. Test results demonstrated that the hysteresis curve of this column was full and it presented superior seismic performance. (Toutanji and Saafi 2001) and (Gupta and Verma 2016) conducted the durability studies on PFCC column and revealed that the specimens had good durability. (Wang 2008, Jiang *et al*. 2014 and Yu *et al*. 2015) established a finite element model for evaluating the mechanical behavior of PFCC column

*Corresponding author, Lecturer
E-mail: fyuan86@126.com
[a]Ph.D.
[b]Student
[c]Student
[d]Ph.D.



ISSN: 1229-9367 (Print), 1598-6233 (Online)

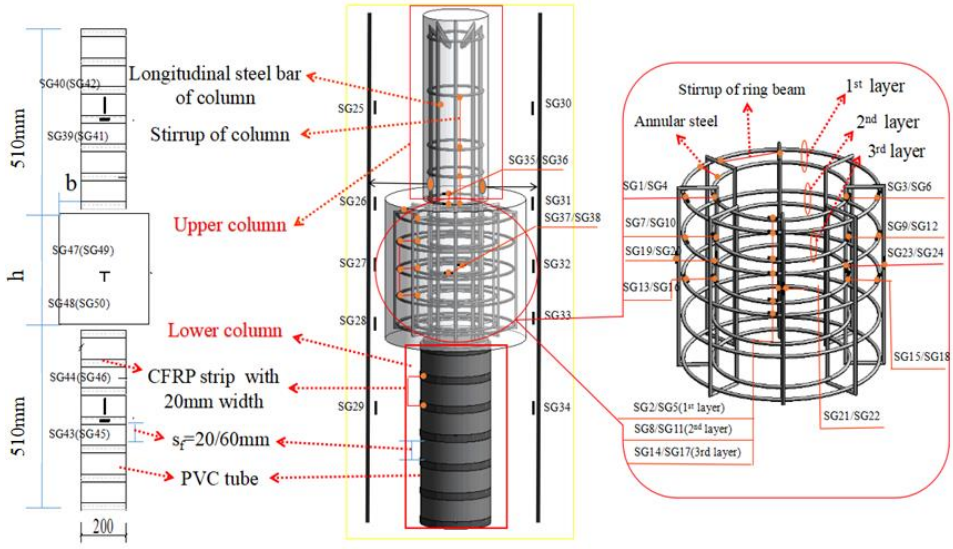


Far from the side of the axial load (T) Near the side of the axial load (C)

Fig. 1 Details of specimens (F7)

Table 1 Parameters of PFCC-RBJs under eccentric compression

| Specimen number | Height of ring beam /$h$ (mm) | Width of ring beam/$b$ (mm) | Reinforcement ratio of ring beam /$\rho$(%) | Eccentricity /$e$(mm) | Layer of FRP / $t_f$ & FRP strip spacing / $s_f$ (mm) | $N_e$ (kN) |
|---|---|---|---|---|---|---|
| F1 | 300 | 75 | 10Φ6.5(1.45%) | 20 | 2/60 | 1005.1 |
| F2 | 300 | 75 | 10Φ6.5(1.45%) | 40 | 2/60 | 753.8 |
| F3 | 300 | 75 | 5Φ6.5+5Φ8 (1.85%) | 20 | 2/60 | 988.9 |
| F4 | 300 | 75 | 10Φ8(2.25%) | 20 | 2/60 | 1012.8 |
| F5 | 300 | 75 | 5Φ6.5+5Φ8 (1.85%) | 40 | 2/60 | 716.7 |
| F6 | 300 | 100 | 4Φ6.5+6Φ8 (1.45%) | 20 | 2/60 | 1126.9 |
| F7 | 300 | 125 | 4Φ6.5+8Φ8 (1.45%) | 20 | 2/60 | 1021.9 |
| F8 | 300 | 100 | 4Φ6.5+6Φ8 (1.45%) | 40 | 2/60 | 787.5 |
| F9 | 240 | 75 | 8Φ6.5(1.45%) | 20 | 2/60 | 990.7 |
| F10 | 180 | 75 | 6Φ6.5(1.45%) | 20 | 2/60 | 1098.5 |
| F11 | 240 | 75 | 8Φ6.5(1.45%) | 40 | 2/60 | 711.6 |
| F12 | 300 | 75 | 5Φ6.5+5Φ8 (1.85%) | 20 | 2/20 | 1227.3 |
| F13 | 300 | 75 | 5Φ6.5+5Φ8 (1.85%) | 20 | - | 908.6 |

Note: *$\rho$ was reinforcement ratio of ring beam, $\rho = \frac{As}{bh}$, in which $A_s$ denoted the total area of annular steel of ring beam; $h$, $b$ represented the ring beam height and width, respectively.

*- indicated that the surface of PVC tube was not wrapped with FRP strips.

* $N_e$ indicated the ultimate carrying capacity of PFCC column.

subjected to axial load. The results showed that PFCC column with the FRP strips spacing of 30 mm-40 mm had good mechanical properties and economic applicability.

In summary, some scholars had carried out many researches on the static performance, seismic performance and durability of PFCC columns. However, few studies were focused on the joint of PFCC column and RC ring beam. Only the author's research group (Zhu 2018, Yu *et al.* 2019) conducted some experimental investigations on the axial compression performance of weak PFCC column and strong RC ring beam joints (PFCC-RBJs). The results showed that the ring beam joint had excellent applicability,

Table 2 Mechanical properties of steel, FRP strips and PVC strips

| Type of materials | Yield strength (MPa) | Tensile strength (MPa) | Elastic Modulus ($10^5$MPa) | Ultimate strain |
|---|---|---|---|---|
| Φ6.5 | 291.30 | 504.30 | 1.93 | - |
| Φ8 | 276.53 | 429.72 | 1.81 | - |
| Φ10 | 350.99 | 553.86 | 1.84 | - |
| CFRP strips | - | 3903 | 2.84 | 0.0137 |
| PVC strips | - | 62.4 | 0.0257 | - |

appreciable carrying capacity and favorable ductility in PFCC structure system. However, the eccentrically compression column was inevitable in practical engineering, and there is no published study on the PFCC-RBJs under eccentric compression.

Therefore, one weak PVC confined concrete column-RC strong ring beam joint (PCC-RBJ) and twelve PFCC-RBJs under eccentric compression were investigated. The effect of five key parameters, such as reinforcement ratio, width and height of ring beam, FRP strips spacing and eccentricity, on the ultimate carrying capacity and strain behavior were analyzed and discussed. Additionally, a modified stress-strain model for conveniently predicting the weak PFCC column and strong RC ring beam joint under eccentric compression was proposed.

### *2.2 Material properties*

The concrete with strength grade C30 was adopted in the experiment. According to the Chinese code GB/T 50081-2002 (GB/T 50081; 2002), the average compressive strength of concrete was 23.6 MPa, and the elastic modulus was $2.43\times10^4$ MPa. The mechanical properties of the steel, FRP strips and PVC tube were respectively determined depending on the Chinese code GB/T 228.1-2010 (GB/T 228.1; 2010), GB/T 3354-2014 (GB/T 3354; 2014) and GB/T 8804.1-2003 (GB/T 8804.1; 2003). The tensile strength of CFRP strips and PVC strips were 3903 MPa and 62.4 MPa respectively. The detailed mechanical properties of steel, FRP strips and PVC tube were listed in Table 2.

### *2.3 Measurement scheme*

#### *2.3.1 Strain gauge arrangement*

To measure the strain of annular steel of ring beam, several strain gauges (SGs), such as SGs1-18, were attached on the compression side (C), the tension side (T) and the symmetry axis (M), as shown in Fig. 1. For the specimens (i.e., F1-F8, F12-F13) with 5 layers or 6 layers of annular steel, SGs were arranged on the 3 layers of annular steel at the upper part of the joint. For the specimens (i.e., F9-F11) with 3 layers or 4 layers of annular steel, SGs were pasted on the 2 layers of annular steel at the upper part of the joint. SGs (i.e., SGs19-24) were attached to the middle of the outer and inner limbs of the stirrup on the side T, M and side C to determine the stirrup strain of ring beam.

To accurately measure the strain of longitudinal steel bars of column, some SGs (i.e., SGs25-34) were arranged on two longitudinal steel bars of the side C and side T. The specific arrangement of SGs was shown in Fig. 1.

To measure the strain of PVC tube, FRP strips and concrete in the joint zone, several SGs were attached to the symmetrical position of the side C and side T of the middle part of the PVC-FRP tube. Eight SGs (i.e., SGs39-46), as depicted in Fig.1, were arranged on PVC-FRP tube to determine the circumferential strain of FRP strips and axial strain of PVC tube, respectively. Additional four SGs (i.e., SGs35-38) were adopted to measure strain stirrup of column at the connection of PFCC column and joint. Two pairs SGs (arranged at 90°), such as SGs47-50, were employed to monitor the axial and circumferential strain of concrete in the side T and side C of specimen at the middle height of joint.

#### *2.3.2 Arrangement of displacement gauges*

A total of 5 displacement gauges (Nos.1-5) were arranged for the specimen, among which No. 1 and No. 2 were used to measure the axial displacement of the specimen. No. 3 was employed to determine the lateral displacement of concrete in joint zone, and No. 4 and No. 5 were adopted to monitor the deflection of the side T in middle of the upper and lower PFCC columns. More details were depicted in Fig. 2.

### *2.4 Loading scheme*

The experiments of PCC-RBJ and PFCC-RBJs under eccentric compression were conducted by the 5000 kN electron-hydraulic servo compressive machine in Structure and Earthquake Resistance Laboratory of Anhui University of Technology, as shown in Fig. 2. Two knife-edge bearings were employed to simulate the boundary conditions of the specimen. The preloading with 5% of the estimated ultimate strength of specimen was firstly applied to check whether the device operated normally. After that, multi-stage load-controlled scheme was applied and the load increment of each stage was 10% of the estimated ultimate strength, and each stage was kept for 2 minutes. When the load increased

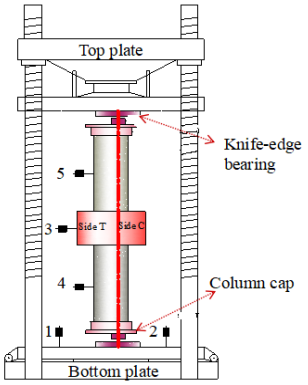


(a) Experimental loading schematic diagram

(b) Experimental loading device diagram

Fig. 2 Test set up

(a) Overall failure mode

(b) Failure mode of PFCC column

(c) Failure mode of joint zone

Fig. 3 Typical failure mode of PFCC-RBJ

to approximately 90% of the estimated ultimate strength of specimen, the displacement-controlled scheme with a constant rate of 0.5 mm/min was employed. The experiment was terminated when the specimen was damaged or the load declined to 85% of the ultimate strength. When the failure of column occurred or the load-displacement curve came into the descent section, and the load fell to 85% of the ultimate strength, the specimen was considered to be damaged.

## 3. Experimental results and analysis

### *3.1 Failure mode*

Three stages, such as the elastic stage, crack development stage, and destruction stage, were observed in the test process of specimen. The variation of appearance was not obvious in elastic stage. With the increase of load, horizontal cracks appeared in the side T of core concrete in the middle of column, and the specimen entered the crack development stage. When the load was close to the ultimate carrying capacity, an obvious flexural deformation appeared on the PFCC column, several FRP strips were broken, and the specimen entered the destruction stage. At this stage, the longitudinal steel in the joint zone yielded, whereas the annular steel in the joint zone not yielded. By comparison, the strain of concrete and stirrup in joint was relatively small, and no visible cracks appeared on the surface of the joint zone. According to the test process and phenomenon, the failure mode of the specimen was ductile failure. The typical failure mode of PFCC-RBJ was depicted in Fig. 3.

### *3.2 Ultimate carrying capacity of PFCC-RBJ*

The carrying capacity was the key property of structural members. In extant studies, the effects of the variable parameters (i.e., $\rho$, b, h, $S_f$, e) on the ultimate carrying capacity was depicted in Fig. 4. The detailed experimental results of ultimate carrying capacity was listed in Table 1.

As illustrated in Figs. 4(a)-4(c), obviously, the reinforcement ratio, width and height had no remarkable impact on the ultimate carrying capacity. This is mainly because, according to the design principle, the damage of the PFCC column in extant studies dominated the failure of the specimen. The reinforcement ratio, width and height had little effect on the ultimate carrying capacity of PFCC column. The ultimate carrying capacity declined with the increase of FRP strips spacing, as shown in Fig. 4(d). This was mainly because the confinement effect of FRP strips on PFCC column weakened as the FRP strips spacing increased. The increase of eccentricity would significantly decrease the ultimate carrying capacity, as demonstrated in Figs. 4(e1)-4(e4). Take specimens F6 (e = 20 mm) and F8 (e = 40 mm) for instance, the carrying capacity of F6 was 1.43 times than that of F8.

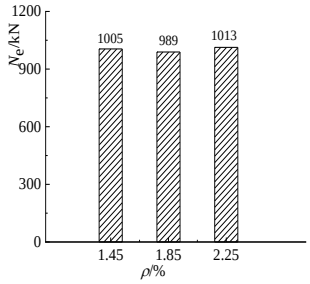


(a) Effect of reinforcement ratio of ring beam

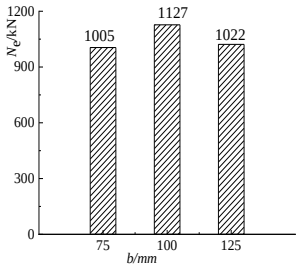


(b) Effect of width of ring beam

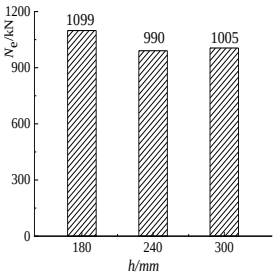


(c) Effect of height of ring beam

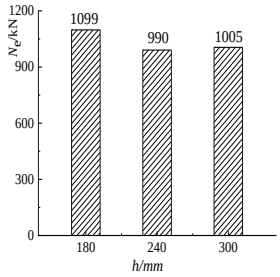


(d) Effect of FRP strips spacing

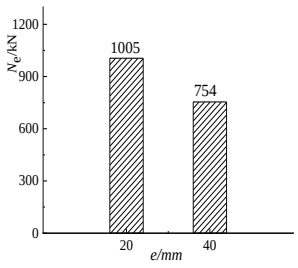


(e1) Effect of eccentricity with $\rho = 1.45\%$

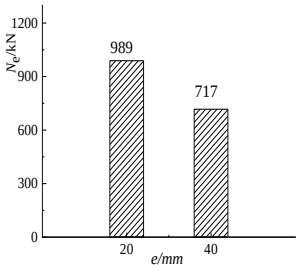


(e2) Effect of eccentricity with $\rho = 1.85\%$

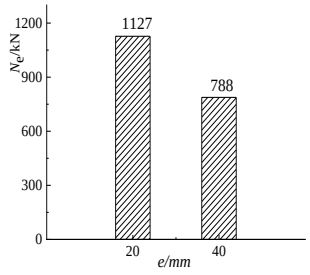


(e3) Effect of eccentricity with $b$=100 mm

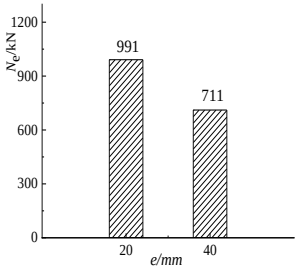


(e4) Effect of eccentricity with $h$=240 mm

Fig. 4 Effect of several parameters on the ultimate carrying capacity

### *3.3 Strain analysis*

#### *3.3.1 Axial strain of PVC tube*

Consistent with the impact on ultimate carrying capacity, three studied parameters (i.e., ρ, b, h,) had no significant effect on the axial strain of PVC tube, and the load-strain curves of specimen were basically identical, as demonstrated in Figs. 5(a)-5(c).

The effect of FRP strips spacing and eccentricity on axial strain of PVC tube was depicted in Figs. 5(d), 5(e1)-5(e4). Initially, as the confinement of FRP strips on PVC tube was very small, the effect of FRP strips spacing on the axial strain of PVC tube was not obvious. With the increment of load, the axial strain of PVC tube decreased with the decrease of FRP strips spacing. It can be concluded that the decrease of eccentricity would slow down the development of axial strain of PVC tube.

#### *3.3.2 FRP strips strain*

As three studied parameters such as reinforcement ratio, width and height were mainly related to joint, the effect of these parameters on the strain of FRP strips was not distinct, as depicted in Figs. 6(a)-6(c).

Fig. 6(d) illustrated the effect of FRP strips spacing on FRP strips strain. The strain of FRP strips decreased with the decrease of FRP strips spacing. In contrast, the impact of FRP strips spacing on the strain of FRP strips on the side C was more obvious than that of side T.

The effect of the eccentricity on the FRP strips strain was depicted in Figs. 6(e1)-6(e4). It can be seen that the increase of eccentricity would accelerate the strain development of the FRP strips. Besides, the effect of eccentricity on accelerating strain development was more significant on side C than that of on side T.

#### *3.3.3 Annular steel strain*

The load-strain relationship curves of annular steel were illustrated in Fig. 7. Clearly, as the confinement effect provided by the inner annular steel was more obvious than that of the outer annular steel, the strain of inner annular steel was larger than that of the outer annular steel at the same layer. The strain of annular steel decreased from middle of joint to the end of joint in the axial direction. In addition, the strain of annular steel on side C was greater

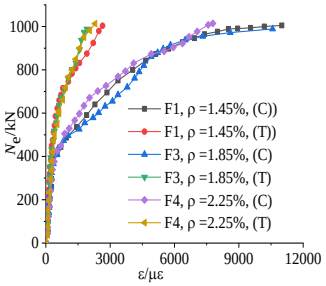


(a) Effect of reinforcement ratio of ring beam

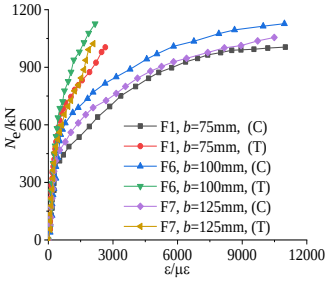


(b) Effect of width of ring beam

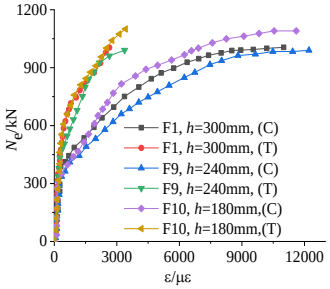


(c) Effect of height of ring beam

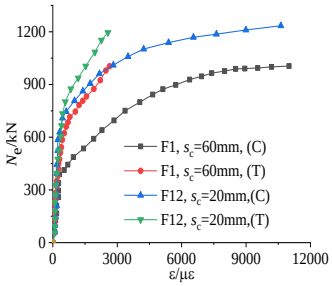


(d) Effect of FRP strips spacing

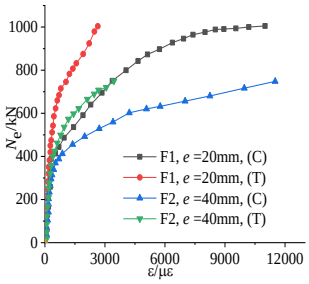


(e1) Effect of eccentricity with $\rho = 1.45\%$

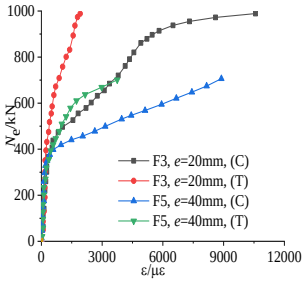


(e2) Effect of eccentricity with $\rho = 1.85\%$

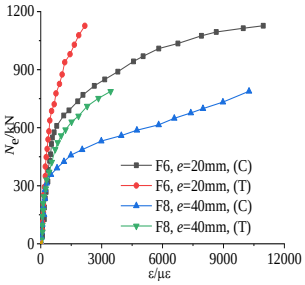


(e3) Effect of eccentricity with $b$=100 mm

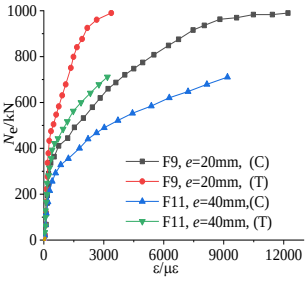


(e4) Effect of eccentricity with h=240 mm

Fig. 5 Effect of several parameters on the axial strain of PVC tube

than that on side T. The confinement effect of annular steel on side C was greater than that of side T.

The effect of reinforcement ratio, width and height on strain of annular steel was depicted in Figs. 8(a)-8(c). With the increase of the reinforcement ratio, width or the decrease of height, the strain development rate of the annular steel on the side C was significantly reduced, while the effect of these three parameters on the strain of the annular steel at the side T was not obvious. As can be seen from Fig. 8(d), the decrease in FRP strips spacing improved the maximum strain of annular steel. This may come from that the ultimate carrying capacity enhanced with the decrease of FRP strips spacing, thereby, the circumferential confinement required by the joint core also increased correspondingly. With the increase of eccentricity, the strain development rate of the annular steel on the side C was significantly reduced, while the eccentricity had little effect on the strain of the annular steel on the side T, as shown in Figs. 8(e1)-8(e4).

### *3.3.4 Ring beam stirrup strain*

The load-strain relationship curves of ring beam stirrup were depicted in Fig. 9. Initially, for the side T of ring beam stirrup, the ring beam stirrup was under compression and the strain of the stirrup developed slowly. The development rate of the inner limbs strain of the stirrup was greater than that of the outer limbs stirrup strain. As the load increased, the compression strain of the stirrup decreased, and the strain of stirrup gradually changed from compression strain to tension strain. For the side C of ring beam stirrup, the ring beam stirrup of specimens with an eccentricity of 20 mm were always under compression, and the strain development rate of the stirrup on side C was larger than that of the stirrup on side T. This may come from that concrete on the side C subjected to the diffusion compressive stress was greater than that of side T. While most of the specimens with an eccentricity of 40 mm were always in a tension state.

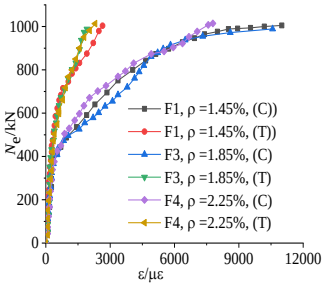


(a) Effect of reinforcement ratio of ring beam

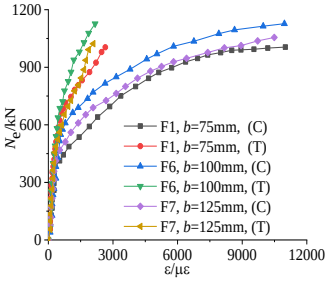


(b) Effect of width of ring beam

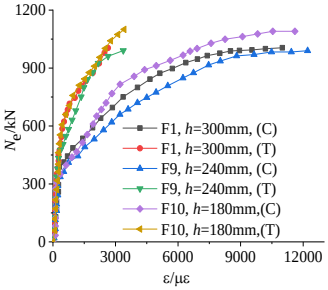


(c) Effect of height of ring beam

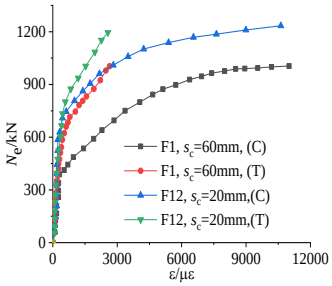


(d) Effect of FRP strips spacing

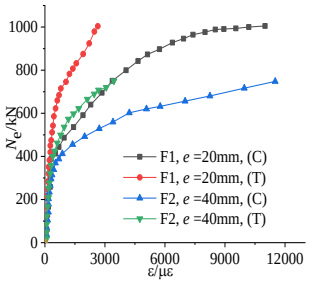


(e1) Effect of eccentricity with $\rho = 1.45\%$

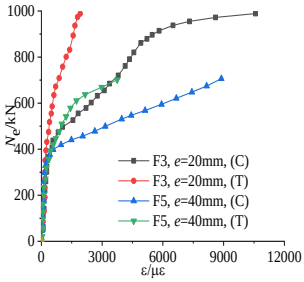


(e2) Effect of eccentricity with $\rho = 1.85\%$

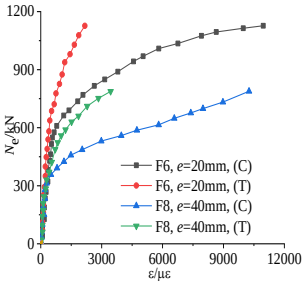


(e3) Effect of eccentricity with $b$=100 mm

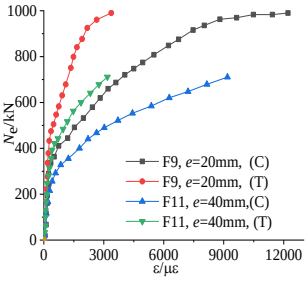


(e4) Effect of eccentricity with $h$=240 mm

Fig. 6 Effect of several parameters on the strain of FRP strips

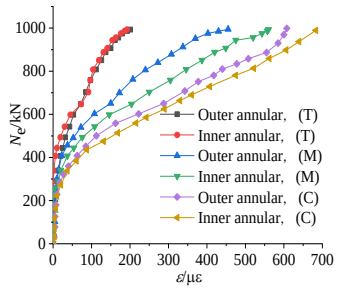


(a)1st layer (F1)

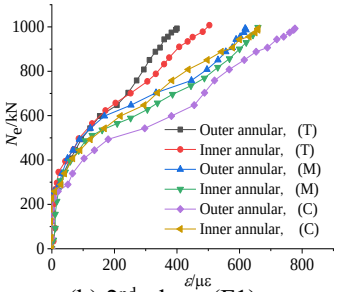


(b) 2nd layer(F1)

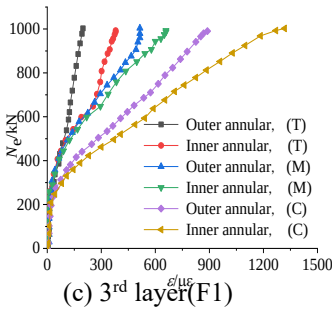


(c) 3rd layer(F1)

Fig. 7 Annular steel strain

As shown in Figs.10 (a1-a2), the strain development rate of the inner limbs decreased, with the reinforcement ratio increased, while the effect of reinforcement ratio on strain development rate of outer limbs was not distinct. With the increase of width, the ring beam stirrup strain development rate of the outer limbs on the side C decreased. During the whole loading process, width had no remarkable impact on ring beam stirrup strain on side T, as shown in Figs .10(b1)-10(b2). In addition, the influence of height on the strain of ring beam stirrup was depicted in Figs. 10(c1)-10(c2). It can be seen that as height decreased, the stirrup strain development rate of the inner limbs on the side T decreased.

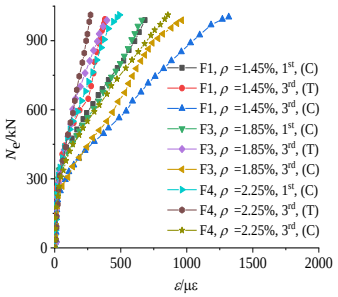


(a) Effect of reinforcement ratio of ring beam

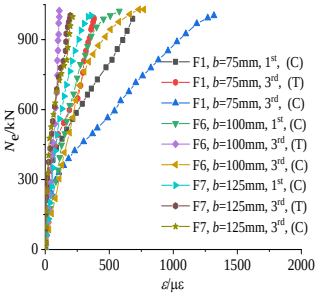


(b) Effect of width of ring beam

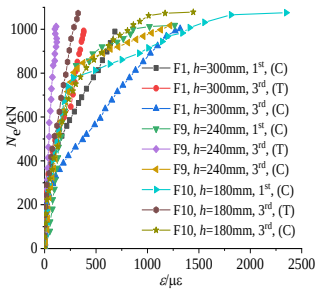


(c) Effect of height of ring beam

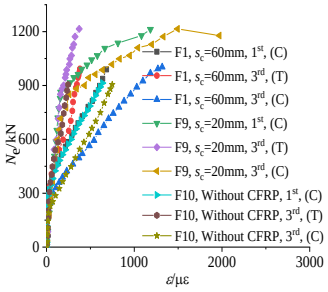


(d) Effect of FRP strips spacing

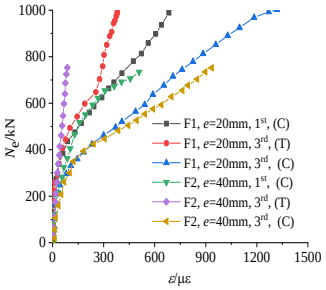


(e1) Effect of eccentricity with $\rho = 1.45\%$

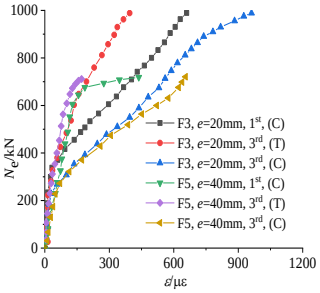


(e2) Effect of eccentricity with $\rho = 1.85\%$

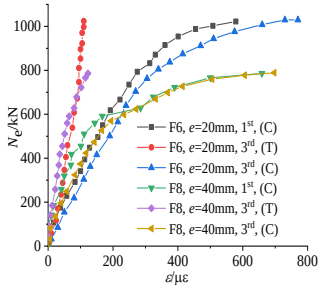


(e3) Effect of eccentricity with $b$=100 mm

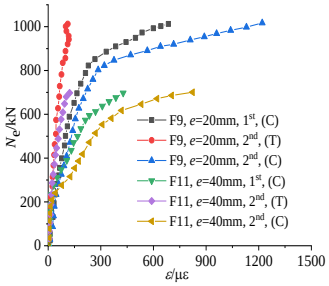


(e4) Effect of eccentricity with $h$=240 mm

Fig. 8 Effect of several parameters on the annular steel strain

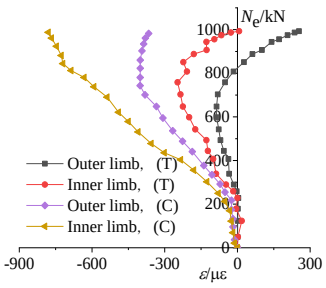


Fig. 9 Stirrup strain of ring beam(F1)

The stirrup strain of the outer limbs on the side T changed from compressive strain to tensile strain with the decrease of the ring beam height. Obviously, the maximum stirrup tensile strain on the side T and the maximum stirrup compressive strain on the side C increased as FRP strips spacing decreased, as illustrated in Figs. 10(d1)-10(d2).

This was mainly because the decrease of FRP strips spacing would enhance the ultimate carrying capacity of specimen, correspondingly improve the stress of ring beam stirrup. As shown in Figs.10(e1)-10(e4), in the initial loading stage, the ring beam stirrup strain increased approximately linearly. As the eccentricity increased, the ring beam stirrup compressive strain development rate on the side T decreased. Compared with the specimens with an eccentricity of 20 mm, the ring beam stirrup of specimens with an eccentricity of 40 mm on the side C were under tension.

## 4. Stress-strain relationship analysis

In this section, the influences of five parameters (i.e., ρ, b, h, $S_f$ , e) on stress-strain relationship of PFCC column were shown in Figs. 11. In these figures, $\sigma_c$ and $\varepsilon_c$ represented the compressive stress and strain of PFCC column, respectively. All the stress- strain curves were

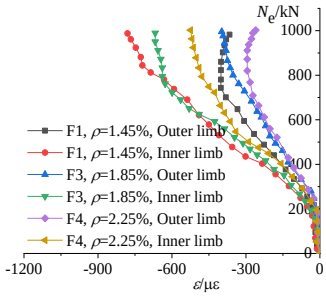


(a1) Effect of reinforcement ratio on side T

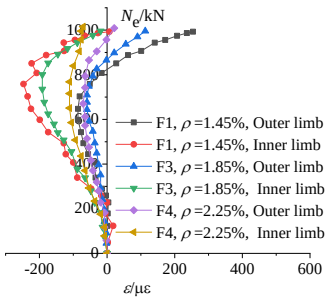


(a2) Effect of reinforcement ratio on side C

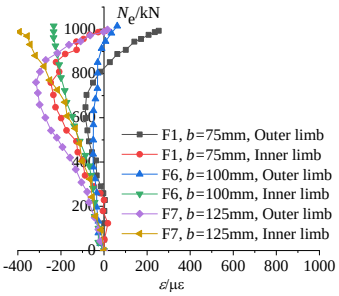


(b1) Effect of width on side T

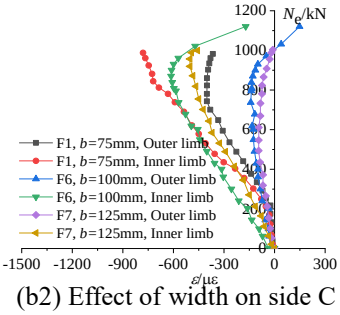


(b2) Effect of width on side C

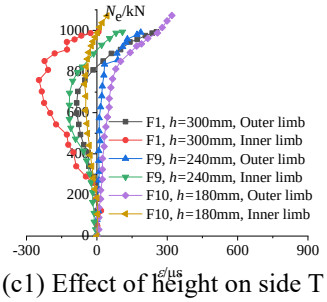


(c1) Effect of height on side T

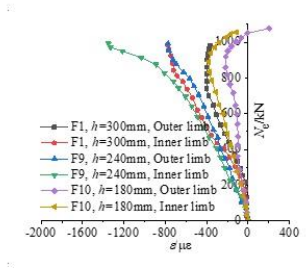


(c2)Effect of height on side C

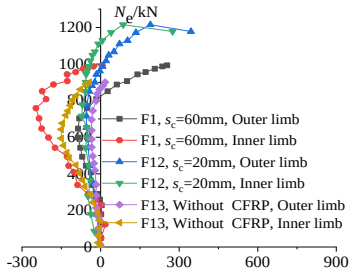


(d1) Effect of FRP strip spacing on side T

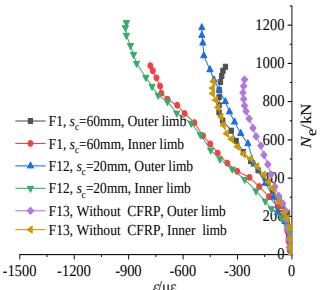


(d2) Effect of FRP strip spacing on side C

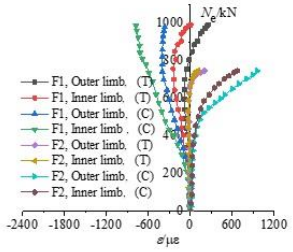


(e1)Effect of eccentricity with $\rho$=1.45%

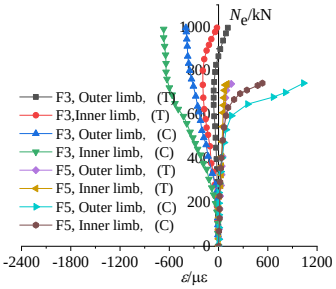


(e2) Effect of eccentricity with $\rho$=1.85%

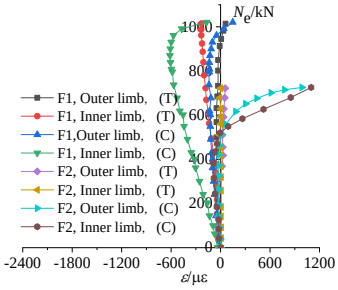


(e3) Effect of eccentricity with $b$=100 mm

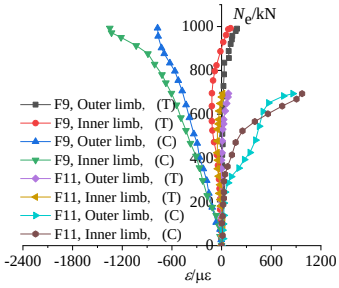


(e4) Effect of eccentricity with $h$=240 mm

Fig. 10 Effect of several parameters on the stirrup strain of ring beam

approximately composed of two stages. The first stage was a parabola, and the second stage was approximately a straight line.

Obviously, during the whole loading process, the reinforcement ratio, width and height had no significant effect on stress-strain relationship curve of PFCC column, as shown in Figs. 11(a1)-11(c2). The main reason was that, as mentioned above, the influence of these three parameters on the strength of PFCC column was not significant. Figs. 11(d1) and 11(d2) depicted the effect of FRP strips spacing on stress-strain relationship curve of PFCC column. It can be seen that the slope of the stress-strain relationship curve decreased with the increment of FRP strips spacing. The ultimate stress and ultimate strain of the PFCC column decreased as the FRP strips spacing increased. As shown in Figs. 11(e11)-11(e42), the slope of the stress-strain relationship curve of the PFCC column decreased with the increase of the eccentricity. The ultimate stress of PFCC column decreased as the eccentricity increased, while the effect of eccentricity on the ultimate strain of PFCC was not distinct.

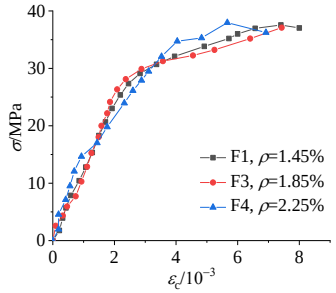


(a1) Effect of reinforcement ratio on upper column

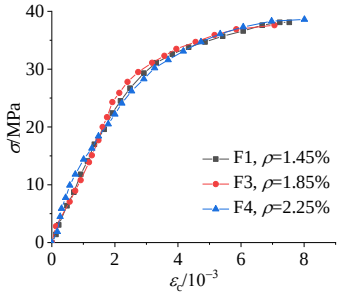


(a2) Effect of reinforcement ratio on lower column

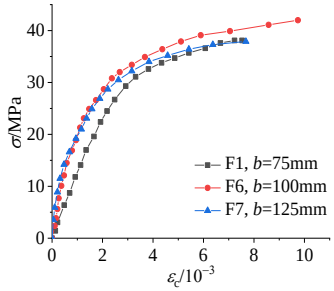


(b1) Effect of width on upper column

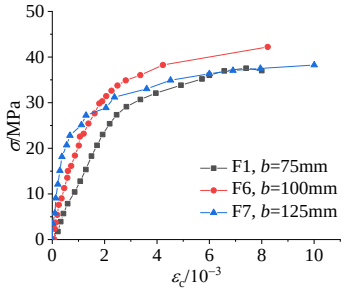


(b2) Effect of width on lower column

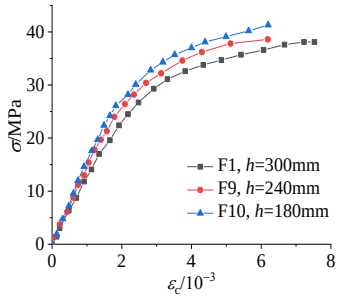


(c1)Effect of height on upper column

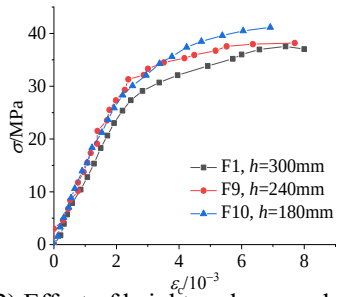


(c2) Effect of height on lower column

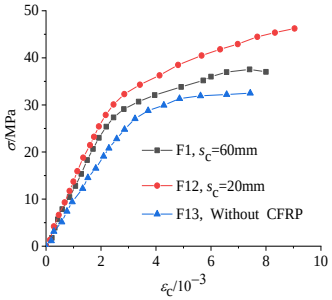


(d1) Effect of FRP strips spacing o n upper column

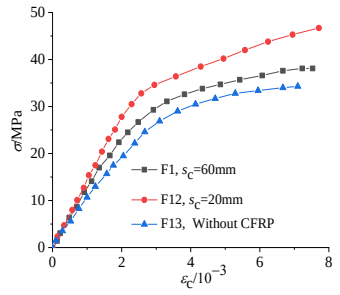


(d2) Effect of FRP strips spacing on lower column

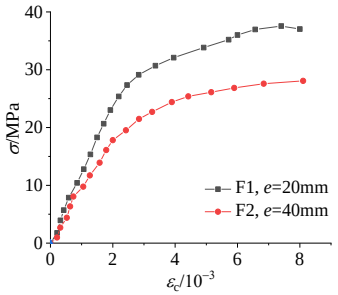


(e11) Effect of eccentricity on upper column with $\rho = 1.45\%$

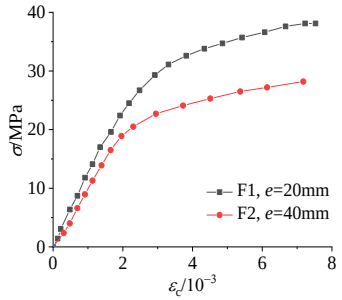


(e12) Effect of eccentricity on lower column with $\rho = 1.45\%$

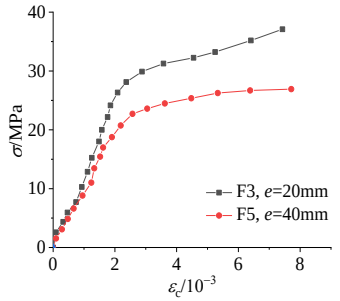


(e21) Effect of eccentricity on upper column with $\rho = 1.85\%$

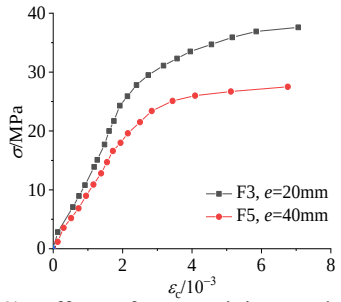


(e22) Effect of eccentricity on lower column with $\rho = 1.85\%$

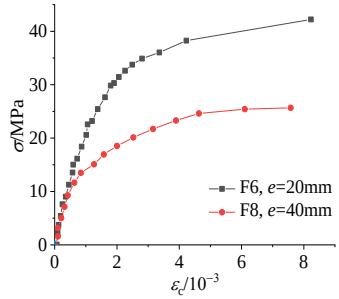


(e31) Effect of eccentricity on upper column with $b = 100\text{mm}$

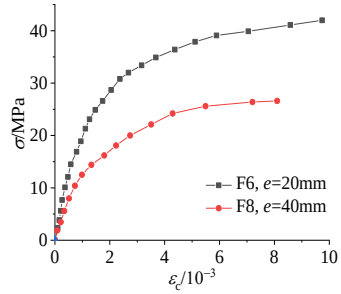


(e32) Effect of eccentricity on lower column with $b = 100\text{mm}$

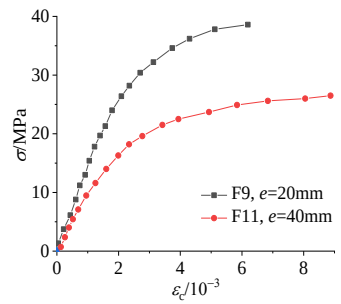


(e41)Effect of eccentricity on upper column with $h = 240\text{mm}$

Continued-

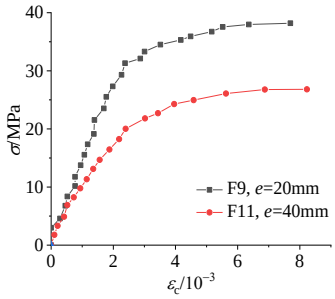


(e42) Effect of eccentricity on lower column with $h = 240\text{mm}$

Fig. 11 Effect of several parameters on the stress-strain curve of PFCC column

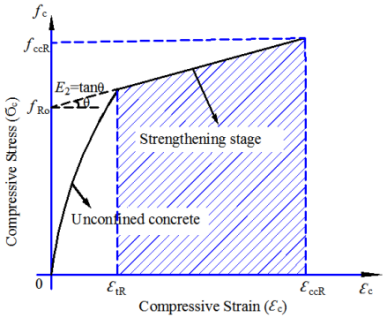


Fig. 12 Typical stress-strain curve of PFCC column

## 5. A model for predicting the stress-strain relation of PFCC-RBJ under eccentric compression

The experimental results showed that different from the uniform confining of concrete under axial load, the confinement of concrete under eccentric compression was not uniform. The confining force decreased with the increase of eccentricity. Considering the effect of eccentricity on the stress-strain relationship, a reduction coefficient of confinement effect $K_z$ was introduced in extant studies, and then a modified stress-strain model for predicting the PFCC-RBJ under eccentric compression was proposed based on the Yu's model (Yu 2007) as shown in Fig. 12.

$$\sigma_c = \begin{cases} 0.58E_c\varepsilon_c - \dfrac{(E_c - E_2)^2}{12 f_{Ro}}\varepsilon_c^{\,2} & 0 \le \varepsilon_c \le \varepsilon_{tR} \\ f_{Ro} + E_2\varepsilon_c & \varepsilon_{tR} \le \varepsilon_c \le \varepsilon_{ccR} \end{cases} \quad (1)$$

In which, $\sigma_c$, $\varepsilon_c$ represented the compressive stress and strain of PFCC column under eccentric compression, respectively. $E_2$ denoted the slope of intensified segment, as determined by Eq. (2). $\varepsilon_{tR}$ was the intersection of the parabola and the intensified segment, as calculated by Eq. (3). $f_{Ro}$ indicated the intercept of the straight line of the intensified section of the PFCC column under compression, as expressed by Eq. (4).

$$E_2 = \frac{f'_{ccR} - f_{Ro}}{\varepsilon'_{cc\,R}} \quad (2)$$

$$\varepsilon_{tR} = \frac{3 f_{Ro}}{(E_c - E_2)} \quad (3)$$

$$f_{Ro} = f_o + k_a \frac{N_s}{A_c} \quad (4)$$

In which, $f'_{ccR}$ indicated the ultimate compressive strength of PFCC column under eccentric compression, as calculated by Eq. (5). $\varepsilon'_{ccR}$ represented the ultimate compressive strain of PFCC column under eccentric compression, as determined by Eq. (6). $f_o$ indicated the intercept of the straight line of the intensified segment of the PFCC column under eccentric compression without reinforcement, as determined by Eq. (7). $N_s$ was the calculated value of carrying capacity of the steel, which can be determined by Eq. (8), where, $A'_s$ was the total area of longitudinal steel in the column, $f'_y$ was the yield strength of longitudinal steel in the column, $k_a = \frac{f'_{ccR}}{f'_{cc}}$ and $k_b = \frac{\varepsilon'_{ccR}}{\varepsilon'_{cc}}$ were the enhancement coefficient of the axial strain and stress of PFCC column, respectively, as listed in Table 3. $\varepsilon'_{cc}$ represented the ultimate compressive strain of PFCC column without reinforcement, $f'_{cc}$ was the ultimate compressive strength of PFCC column without reinforcement.

$$f'_{ccR} = k_a f_c\left(1 + 1.31\xi'_{ef}\right) \quad (5)$$

$$\varepsilon'_{ccR} = 0.0111 + 0.0077\xi'_{ef} \quad (6)$$

$$f_o = 24.734\left(\xi'_{ef}\right)^{-0.0692} \quad (7)$$

$$N_s = f'_y\, A'_s \quad (8)$$

$$\xi'_{ef} = k_z \xi_{ef} \quad (9)$$

Table 3 Test values of $k_a$ and $k_b$

| Data Sources | Specimen number | $f'_{cc}$ | $f'_{ccR}$ | $\varepsilon'_{cc}$ | $\varepsilon'_{ccR}$ | $k_a$ | $k_b$ |
|---|---|---|---|---|---|---|---|
| Yu | AR-Cs20 | 56.85 | 65.06 | 0.0172 | 0.0199 | 1.14 | 1.16 |
| | AR-Cs30 | 47.99 | 58.31 | 0.0159 | 0.0172 | 1.22 | 1.08 |
| | AR-Cs40 | 44.24 | 56.59 | 0.0147 | 0.0169 | 1.28 | 1.15 |
| | AR-Cs50 | 40.64 | 52.71 | 0.0135 | 0.0166 | 1.30 | 1.23 |
| | AR-Cs60 | 41.21 | 50.96 | 0.0129 | 0.0146 | 1.24 | 1.13 |
| Wang 2016 | AR2-Bs20 | 36.81 | 36.94 | 0.0055 | 0.0092 | 1.00 | 1.67 |
| | AR2-Bs30 | 34.73 | 35.73 | 0.0050 | 0.0080 | 1.03 | 1.60 |
| | AR2-Bs40 | 34.24 | 35.10 | 0.0049 | 0.0062 | 1.03 | 1.27 |
| | AR2-Bs50 | 34.07 | 33.69 | 0.0047 | 0.0060 | 0.99 | 1.28 |
| | AR2-Bs60 | 32.28 | 37.01 | 0.0045 | 0.0069 | 1.15 | 1.53 |
| Average value | | | | | | 1.14 | 1.31 |

In which, $\xi'_{ef}$ represented the equivalent confinement effect coefficient of PFCC column under eccentric compression, $\xi_{ef}$ denoted the confinement effect coefficient of axially loaded PFCC column, $\xi_{ef}=\frac{A_f f_f}{A_c f_c}k_g$, $A_f$ was the area of FRP strips, $A_f=\pi d t_f$. $k_g$ was the confinement effect coefficient of FRP strips, $k_g=\frac{S_f}{S'_f}$, $s_f$ and $s'_f$ were the width and spacing of the FRP strips, respectively, $s'_f \geq s_f$.

$k_z$ represented the reduction coefficient of confinement effect, which was fitted by the regression analysis of test data, as shown in Fig. 13 and Eq. (10).

$$k_z = -1.441\left(\frac{2e}{d}\right)^2 - 0.208\left(\frac{2e}{d}\right)+1 \quad (10)$$

The comparison between the stress-strain curves predicted by the proposed model and the measured stress-strain curves were depicted in Fig. 14. It can be seen that the proposed model were in good agreement with the test data.

## 6. Conclusions

One PCC-RBJ and twelve PFCC-RBJs under eccentric compression were designed with principle of "strong joint and weak column" and tested in extant studies. Several key parameters including width, height and reinforcement ratio of ring beam, eccentricity and FRP strips spacing were considered. The following conclusions can be drawn.

- The failure mode of the PFCC-RBJs under eccentric compression was the broken of several FRP strips, the cracking of PVC tube and the concrete on the side C of the PFCC was crushed.
- The ultimate carrying capacity of eccentrically loaded PFCC-RBJ decreased as the FRP strips spacing or eccentricity increased. The effect of the reinforcement ratio, width and height of ring beam on the ultimate carrying capacity was not obvious.
- The axial strain of PVC tube decreased as the FRP strips spacing decreased. The decrease of eccentricity would slow down the development of axial strain of the PVC tube. Other three studied parameters had little effect on the axial strain of the PVC tube.
- The strain of the FRP strips decreased with the increase of FRP strips spacing. The increase of eccentricity would accelerate the strain development of the FRP strips. Reinforcement ratio, width and height of ring beam had little effect on the strain of the FRP strips.
- The slope of the stress-strain curve of PFCC column decreased as the FRP strips spacing or eccentricity increased. The ultimate strain of the PFCC column decreased as the FRP strips spacing increased, while the effect of eccentricity on the ultimate strain of PFCC was not distinct. Other three studied parameters had no evident effect on the stress-strain curve of PFCC column.
- Considering the influence of eccentricity on the stress-strain relationship, a reduction coefficient of confinement effect $k_z$ was introduced, and then a modified stress-strain model for predicting the weak PVC-FRP confined concrete column and strong RC ring beam joint

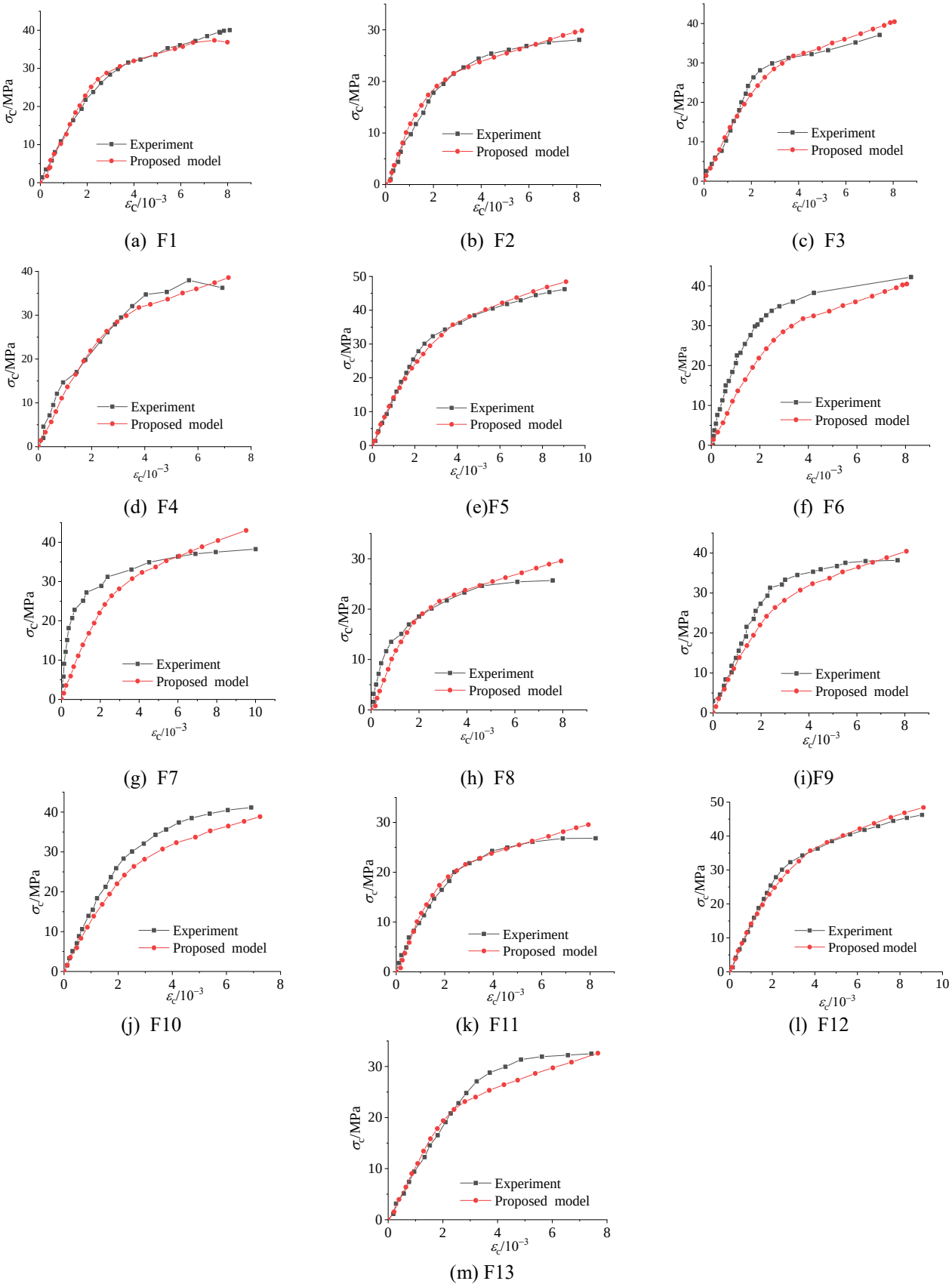


(a) F1 (b) F2 (c) F3

(d) F4 (e)F5 (f) F6

(g) F7 (h) F8 (i)F9

(j) F10 (k) F11 (l) F12

(m) F13

Fig. 14 Comparison of stress-strain curves for joint between proposed model and test data

under eccentric compression was proposed. The proposed model agreed well with the test data.

## Acknowledgements

This research was supported by National Natural Science Foundation of China (Nos. 51878002, 51578001, 51608003 and 51008001), Ministry of Housing and Urban-Rural Development (No.2012-K2-7), Key Research and Development Plan of Anhui Province (No.1704a0802131), and the Outstanding Young Talent Support Program of Anhui Province (No. gxyqZD2016072).

## References

Abdelkarim, O.I., ElGawady, M.A., Anumolu, S., Gheni, A. and Sanders, G.E. (2017), "Behavior of hollow-core FRP - concrete-steel columns under static cyclic flexural loading", *J. Struct. Eng. - ASCE*, **144**(2), 04017188. https://doi.org/10.1061/(ASCE)ST.1943-541X.0001905.

Attari, B. and Tavakkolizadeh, M. (2019), "An experimental investigation on effect of elevated temperatures on bond strength between externally bonded CFRP and concrete", *Steel Compos. Struct.*, **32** (5), 559-569. https://doi.org/10.12989/scs.2019.32.5.559.

Chen, B.L. and Wang, L.G. (2019), "Experimental study on flexural behavior of splicing concrete-filled GFRP tubular composite members connected with steel bars", *Steel Compos. Struct.*, **18** (5), 1129-1144. https://doi.org/10.12989/scs.scs.2015.18.5.1129.

Chen, J.F. and Teng, J.G. (2001), "Anchorage Strength Models for FRP and Steel Plates Bonded to Concrete", *J. Struct. Eng.-ASCE,* **127**(7), 784-791. https://doi.org/10.1061/(ASCE)07339445(2001)127:7(784).

Dhahir, M.K. (2017), "Shear strength of FRP reinforced deep beams without web reinforcement", *Compos. Struct.*, **165**, 223-232. https://doi.org/10.1016/j.compstruct.2017.01.039.

Fakharifar, M. and Chen, G. (2016), "Compressive behavior of FRP-confined concrete-filled PVC tubular columns", *Compos. Struct.*, **141**, 91-109. https://doi.org/10.1016/j.compstruct.2016.01.004.

Fakharifar, M. and Chen, G. (2017), "FRP-confined concrete filled PVC tubes: A new design concept for ductile column construction in seismic regions", *Constr. Build. Mater.*, **130**, 1-10. https://doi.org/10.1016/j.conbuildmat.2016.11.056.

GB/T228.1 (2010), "Metallic materials - Tensile testing- Part 1: Method of test at room temperature", China.

GB/T3354 (2014), "Test method for tensile properties of orientational fiber reinforced polymer matrix materials", China.

GB/T50081 (2002), "Standard for test method of mechanical properties on ordinary the concrete strength of the concrete", China.

GB/T8804.1 (2003), "Thermoplastic pipes-Determination of tensile properties", China.

Gholampour, A. and Ozbakkaloglu, T. (2017), "Finite Element Analysis of Constitutive Behavior of FRP-Confined Steel Fiber Reinforced Concrete." *Key Eng Mater,* **737**, 511-516. https://doi.org/10.4028/www.scientific.net/KEM.737.511

Grammatikou, S., Biskinis, D. and Fardis, M.N. (2018), "Effect of load cycling, FRP jackets, and lap-splicing of longitudinal bars on the effective stiffness and ultimate deformation of flexure-controlled RC members", *J. Struct. Eng. - ASCE*, **144**(6), 04018056. https://doi.org/10.1061/(ASCE)ST.1943-541X.0002045

Gupta, P.K. and Verma, V.K. (2016), "Study of concrete-filled unplasticized poly-vinyl chloride tubes in marine environment." *Proceedings of the Ins of Mech Eng Part M-J Eng for the Marit Envir,* **230**(2), 229-240. https://doi.org/10.1177/1475090214560448.

Harajli, M.H. (2006), "Axial stress–strain relationship for FRP confined circular and rectangular concrete columns", *Cement Concrete Compos.*, **28**(10), 938-948. https://doi.org/10.1016/j.cemconcomp.2006.07.005.

Jiang, S.F., Ma, S.L. and Zhao, Q.W. (2014), "Experimental study and theoretical analysis on slender concrete-filled FRP - PVC tubular columns", *Constr. Build. Mater.*, **53**(2), 475-487. https://doi.org/10.1016/j.conbuildmat.2013.11.089.

Jiang, S.F. and Ma, S.L. (2014), "Experimental study on hysteretic behavior of circular section reinforced concrete composite columns with FRP-PVC tube", *J. Build. Struct*., **35**(2), 111-118. https://doi.org/10.15951/j.tmgcxb.2014.01.013.

Kurt, C.E. (1978), "Concrete-filled structure plastic columns", *J. Struct. Div.*, **104**(1), 55-63.

Mansouri, I. and Kisi, O. (2015), "Prediction of debonding strength for masonry elements retrofitted with FRP composites using neuro fuzzy and neural network approaches", *Compos. Part B: Eng*., **70**(5), 247-255. https://doi.org/10.1016/j.compositesb.2014.11.023

Mansouri, I. Ozbakkaloglu, T. Kisi, O. and Xie, T. (2016), "Predicting behavior of FRP-confined concrete using neuro fuzzy, neural network, multivariate adaptive regression splines and M5 model tree techniques", *Mater. Struct*., **49**(10), 4319-4334. https://doi.org/10.1617/s11527-015-0790-4.

Niu, D.T., Yu, F. and Wang, Z.W. (2017), "Eccentric compression performance of PVC-CFRP confined reinforced steel tube concrete column", *Acta Mater. Compos. Sinica*, **34**(10), 2356-2366. https://doi.org/10.13801/j.cnki.fhclxb.20170222.002.

Ozbakkaloglu, T. and Lim, J.C. (2013), "Axial compressive behavior of FRP-confined concrete: Experimental test database and a new design-oriented model", *Compos. Part B: Eng.*, **55**(12), 607-634. https://doi.org/10.1016/j.compositesb.2013.07.025..

Ozbakkaloglu, T., Lim, J.C. and Vincent, T. (2013), "FRP-confined concrete in circular sections: Review and assessment of stress–strain models", *Eng. Struct.*, **49**(4), 1068-1088. https://doi.org/10.1016/j.engstruct.2012.06.010.

Prashob, P.S. Shashikala, A.P. and Somasundaran, T.P. (2019), "Characteristics of CFRP strengthened tubular joints subjected to different monotonic loadings", *Steel Compos. Struct.*,**32**(3), 361-372. https://doi.org/10.12989/scs.2019.32.3.361.

Saafi, M. (2001), "Development and behavior of a new hybrid column in infrastructure systems", *Texas: Doctoral Dissertation of the University of Alabama.*

Teng, J.G. Jiang, T. and Lam L. (2009), "Refinement of a design-oriented stress–strain model for FRP-confined concrete", *J. Compos. Constr*., **13**(4), 269-278. https://doi.org/10.1061/(ASCE) CC. 1943-5614.0000012.

Toutanji, H. and Saafi, M. (2001), "Durability studies on concrete columns encased in PVC–FRP composite tubes", *Compos. Struct.*, **54**(1), 27-35. https://doi.org/10.1016/S0263-8223(01)00067-8.

Toutanji, H. and Saafi, M. (2002), "Stress-strain behavior of concrete columns confined with hybrid composite materials", *Mater. Struct.*, **35**(6), 338-347. https://doi.org/10.1007/BF02483153.

Wang, Z.W. (2008), "Study on Mechanical Properties of Axial Compression PVC-FRP tube Concrete Short Column", *Xi'an：Xi'an University of Architecture and Technology.*

Wei, Y.Y. and Wu, Y.F. (2012), "Unified stress-strain model of concrete for FRP-confined columns", *Constr. Build. Mater.*,

**26**(1), 381-392. https://doi.org/10.1016/j.conbuildmat.2011.06.037.

Xie, Q., Sinaei, H., Shariati, M., Khorami, M., Mohamad, E.T. and Bui, D.T. (2019), "An experimental study on the effect of CFRP on behavior of reinforce concrete beam column connections", *Steel Compos. Struct.*, **30**(5), 433-441. https://doi.org/10.12989/scs.scs.2019.30.5.433.

Yu, F. Xu, G.S. and Cheng, A.C. (2016), "Analysis of shear bearing capacity of reinforced concrete columns with pvc-cfrp tubes under low cyclic loading", *J. Build. Struct.*, **37**(11), 106-112. https://doi.org/10.14006/j.jzjgxb.2016.11.014.

Yu, F. Cheng, A.C. Xu, G.S. and Li, D.G. (2015), "Nonlinear finite element analysis of PVC-FRP confined concrete short column under axial compression", *Indust. Constr.*, **45**(4), 77-82.

Yu, F. (2007), "Experimental study and theoretical analysis of mechanical properties of PVC-FRP confined concrete columns." *Xi'an: Xi'an University of Architecture and Technology*.

Yu, F. and Niu D.T. (2010), "Stress-strain model of PVC-FRP confined concrete column subjected to axial compression." *Int. J. Phys. Sci.,* **5**(15), 2304-2309. http://www.academicjournals.org/IJPS.

Yu, F., Li, D.A., Niu, D.T., Zhu, D.F., Kong, Z.Y., Zhang, N.N. and Fang, Y. (2019), "A model for ultimate bearing capacity of PVC-FRP confined concrete column with reinforced concrete beam joint under axial compression", *Constr. Build. Mater.*, **214**, 668-676. https://doi.org/10.1016/j.conbuildmat.2019.04.131.

Yu, F., Xu, G.S., Niu, D.T., Cheng, A.C., Wu, P. and Kong, Z.Y. (2018), "Experimental study on PVC-FRP confined concrete columns under low cyclic loading", *Constr. Build. Mater.*, **177**(20), 287-302. https://doi.org/10.1016/j.conbuildmat.2018.05.111.

Yu, F., Zhang, N.N., Niu, D.T., Kong, Z.Y., Zhu, D.F., Wang, S.L. and Fang, Y. (2019), "Strain analysis of PVC-FRP confined concrete column with ring beam joint under axial compression", *Compos. Struct.*, **224**, 1-14. https://doi.org/10.1016/j.compstruct.2019.111012.

Zhu, D.F. (2018), "Study on axial compression performance of PVC-FRP confined concrete column-reinforced concrete beam joint", *Ma'anshan：Anhui University of Technology.*

*CC*